1 **Body density of humpback whales (*Megaptera novaengliae*) in feeding aggregations**

2 **estimated from hydrodynamic gliding performance**

3

4 Tomoko Narazaki[1, 2*], Saana Isojunno[1], Douglas P Nowacek[3¶], Rene Swift[1¶], Ari S

5 Friedlaender[4¶], Christian Ramp[1,5¶], Sophie Smout[1&], Kagari Aoki[1,2&], Volker B Deecke[6],

6 Katsufumi Sato[2&], Patrick JO Miller[1].

7

8 [1]Sea Mammal Research Unit, University of St Andrews, Fife, United Kingdom

9 [2]Atmosphere and Ocean Research Institute, University of Tokyo, Kashiwa, Chiba, Japan

10 [3]Nicholas School of the Environment and Pratt School of Engineering, Duke University

11 Marine Laboratory, Beaufort, North Carolina, United States of America

12 [4]Institute of Marine Sciences, University of California Santa Cruz, Santa Cruz, California,

13 United States of America

14 [5]Mingan Island Cetacean Study, Longue-Pointe-de-Mingan, Québec, Canada

15 [6]Department of Science, Natural Resources and Outdoor Studies, University of Cumbria,

16 Ambleside, United Kingdom

17

18 *corresponding author

19 Email: naratomoz@gmail.com

20

21 [¶]These authors contributed equally to this work

22 [&]These authors also contribute equally to this work

23

24

Abstract

Many baleen whales undertake annual fasting and feeding cycles, resulting in substantial changes in their body condition, an important factor affecting fitness. As a measure of lipid-store body condition, tissue density of a few deep diving marine mammals has been estimated using a hydrodynamic glide model of drag and buoyancy forces. Here, we applied the method to shallow-diving humpback whales (*Megaptera novaeangliae*) in North Atlantic and Antarctic feeding aggregations. High-resolution 3-axis acceleration, depth and speed data were collected from 24 whales. Measured values of acceleration during 5 s glides were fitted to a hydrodynamic glide model to estimate unknown parameters (tissue density, drag term and diving gas volume) in a Bayesian framework. Estimated species-average tissue density (1031.6 ± 2.1 kg m^{-3}, $\pm95\%$ credible interval) indicates that humpback whale tissue is typically negatively buoyant although there was a large inter-individual variation ranging from 1025.2 to 1043.1 kg m^{-3}. The precision of the individual estimates was substantially finer than the variation across different individual whales, demonstrating a progressive decrease in tissue density throughout the feeding season and comparably high lipid-store in pregnant females. The drag term ($C_D A m^{-1}$) was estimated to be relatively high, indicating a large effect of lift-related induced drag for humpback whales. Our results show that tissue density of shallow diving baleen whales can be estimated using the hydrodynamic gliding model, although cross-validation with other techniques is an essential next step. This method for estimating body condition is likely to be broadly applicable across a range of aquatic animals and environments.

Introduction

The body condition of animals influences survival rate and reproductive success and thereby impacts the dynamics of entire populations. Body condition also affects an animal's behavioural decisions related to foraging, predator avoidance, migration, and reproductive strategies (e.g. [1-3]). Many marine mammals undergo substantial changes in lipid-store body condition as a result of annual fasting and feeding cycles [4, 5]. For migratory species, the cost of reproduction at breeding grounds is supported by energy gained on feeding grounds. Thus, the amount of energy stored during a feeding season strongly influences reproduction via pregnancy rate [6], foetal development [7], body condition and survival of offspring [8-11] and the competitive capabilities of males. It is also likely that body condition influences the foraging decisions made by baleen whales relative to where prey items are located in the water column [12, 13]. Because body condition is an important factor affecting fitness, measuring body condition of free-ranging cetaceans is important for understanding their ecology as well as for designing effective conservation plans [14-16].

Baleen whales (parvorder Mysticeti; order Cetartiodactyla) are a group of marine mammals that cycle fat stores on an annual basis, substantially changing their appearance, behaviour, and fitness [17]. Given these dramatic changes, developing methods to quantify their body condition in the field has great value. Traditional approaches to examine variations in body condition and energy store of baleen whales involved anatomical measurements that were often made in conjunction with whaling operations [4, 18, 19]. Blubber thickness of whale carcasses has been used as a proxy of body condition [4, 18, 20], since most of the energy is stored in the form of blubber [21] although a considerable amount of energy is also stored in muscle and intra-abdominal fat [4, 21]. Blubber lipid content of whale carcasses was also important in the assessment of condition of cetaceans [19]. As the thickness as well as lipid

72 content and fatty acid composition of blubber has been shown to vary across the body of

73 cetaceans, multiple-site measurements of blubber thickness are particularly useful to examine

74 total body condition cetaceans [22-24]. Many studies have investigated seasonal trends in

75 energy storage of several species of baleen whales by means of blubber thickness and

76 morphometric data, reporting that seasonal fattening varies with different sex and age classes,

77 reproductive stages, as well as prey availability [4, 6, 25].

78

79 Although carcasses have provided many insights into the physiology and body condition of

80 baleen whales, a key limitation is that temporal changes of the same individual cannot be

81 measured. Also, studies using carcasses may not be widely applicable to cetaceans because

82 they require lethal sampling or collection of samples from stranded animals or fisheries

83 bycatch. To collect blubber and other tissue samples from free-ranging cetaceans, biopsy

84 darting is commonly used where modified dart tips are delivered using a crossbow or a

85 pneumatic rifle [26]. The percentage lipid content of blubber from carcasses is considered to

86 be an informative measure of fattening [19]. However, the biopsy blubber samples may not be

87 useful to measure body condition of free-ranging cetaceans because the (1) the force of

88 darting can damage adipocytes causing lipids to be squeezed out of samples, or to seep out of

89 blubber biopsies while in seawater [27], and (2) the sample only penetrates a short distance

90 into the blubber layer. In addition, it is difficult to obtain multiple biopsy samples from a

91 whale whose blubber thickness and composition vary across the body [22-24]. Visual

92 assessment of external shape and appearance based on boat-based photographs has been used

93 for evaluating body condition of right and grey whales [28, 29]. Photogrammetric

94 measurements of body width, reflecting blubber thickness, using vertical aerial photographs

95 taken from aircraft or unmanned aerial vehicles has also been used to assess nutritive body

96 condition of some whale species [11, 30, 31] although measurements of such body shape

97   patterns are limited to the visible 2-dimensionall shape of surfacing of whales, and may not be

98   suitable for other more cryptic species.

99

100   An alternative approach is to use body density of diving animals as a proxy of lipid-store

101   body condition [32]. Lipids are less dense than seawater while other non-gas body

102   components are denser than seawater. Body composition, particularly the ratio of lipid to lean

103   tissue, therefore strongly influences body density and hence the buoyancy of diving animals

104   [5]. It has been shown that buoyancy influences swimming behaviour and energetics of diving

105   animals [33]. For instance, buoyancy forces affect stroking efforts [34, 35] and swimming

106   patterns, with more gliding occurring in the direction aided by buoyancy [15, 34, 36-39].

107

108   Buoyancy also influences gliding performance by altering vertical speeds during inactive drift

109   periods [5], prolonged glides [39] or short-duration glides [38]. This effect of buoyancy on

110   gliding performance has led to the development of tag-based methods to quantify the body

111   density of diving animals via hydrodynamic analysis. This approach was first developed for

112   free-ranging elephant seals (*Mirounga* spp.): body density was quantified by analysing the

113   vertical speed during inactive drifting periods (i.e. drift rate) at which the buoyancy force is

114   assumed to be equal to the drag force [5]. The drift dive method has proven useful for long-

115   term monitoring of body lipid-stores in elephant seals providing new insights into when and

116   where they gain or lose lipid stores [5, 40, 41]. However, use of the drift dive method is

117   limited to a few pinniped species that routinely perform drift dives (*Mirounga angustirostris*

118   [34, 42]; *M. leonina* [5, 40]; *Arctocephalus forsteri* [43]; *Cystophora cristata* [44]). Gliding

119   during the descent or ascent phase of a dive, on the other hand, is commonly observed across

120   a range of diving taxa [33, 37]. A more widely applicable approach, the glide model, was

121   introduced by Miller et al. [38] to estimate body density of sperm whales using a

122   hydrodynamic glide model that predicts how drag and buoyancy forces influence acceleration

123   (or deceleration) during short-duration glides. Aoki et al. [34] conducted a validation analysis

124   using isotope dilution and confirmed a strong correspondence in body density estimates of

125   elephant seals obtained from the drift dive and the glide models [45].

126

127   In the glide model, acceleration during a glide is determined by the difference between drag

128   and net buoyancy forces along the swimming path of the animal [38]. The force of non-

129   neutral buoyancy or 'apparent weight' (difference in mass of the diving animal and the

130   displaced water) acts vertically on diving animals, and depends on the density of body tissues

131   as well as the volume of air carried within the body (the diving gas volume). While body

132   tissues are relatively incompressible at depth, the volume of air in the body progressively

133   decreases with increasing depth, thought to closely follow Boyle's Law for marine mammals

134   [46]. Thus, tissue-derived buoyancy can be separated from air-derived buoyancy when gliding

135   data is available over a wide depth range. To date, the glide model has been demonstrated to

136   be useful to estimate the body density of several species of marine mammals, including

137   elephant seals [34] and some deep diving toothed whales (sperm whale, *Physeter*

138   *macrocephalus* [38]; Northern bottlenose whale, *Hyperoodon ampullatus* [15]; long-finned

139   pilot whale, *Globicephala melas* [47]) that routinely perform dives deeper than 200 m where

140   the effect of air-derived buoyancy is considered to be negligible [38].

141

142   In this study, we apply the hydrodynamic glide model to estimate body tissue density of

143   humpback whales (*Megaptera novaeangliae*) in two geographically distinct feeding

144   populations (the Gulf of St Lawrence, Canada and the Western Antarctic Peninsula, WAP). In

145   comparison with deeper diving toothed whales, humpback whales may not seem ideal

146   candidates for the glide model because they routinely dive only to relatively shallow depths at

147   which gas volumes are likely to more strongly influence net buoyancy. For example, the mean

148   dive depth per tag record in this study ranged from 22.8 to 180.8 m, with the deepest dive

149   recorded being 388.3 m. Apart from a shallower diving depth range, humpback whales tend to

150   dive and glide at relatively shallower pitch angles, requiring the generation of lift. The large

151   flippers of humpback whales are well-suited for this purpose [48], but the need to generate

152   substantial lift forces may raise concerns about the applicability of the glide model because

153   the current model does not include the potential effect of lift-induced drag which was shown

154   to be negligible in deep divers that maintain steep pitch during glides [34].

155

156   The objective of this study was to examine whether the hydrodynamic glide model can be

157   applied to shallower diving baleen whales by examining the precision of body density

158   estimates obtained from a narrow depth-range dataset. Our results show that we were able to

159   obtain estimates of humpback whale body density using this method. Though the precision of

160   the estimates was not as fine as was previously reported for a deep-diving toothed whale [15],

161   the precision of individual body density estimates was substantially finer than the variation

162   across different individual whales, including some differences between the geographic

163   locations where tags were attached. We conclude that the glide method has potential to be

164   used to track the body condition of shallow diving baleen whales, enabling future applications

165   as a tool to study their health and how body condition relates to reproductive status, animal

166   behaviour and the influences of environmental change and variability.

167

168 # Materials and methods

169 ## Ethics statement

170 The research protocol was approved by Animal Welfare and Care Committee Approval of the

171 University of St Andrews. The fieldwork in the Gulf of St Lawrence, Canada was performed

172 under permits issued by the Research permits issued by Department of Fisheries and Oceans,

173 Canada (scientific fishing license QUE04-B-2011) in compliance with ethical and local use of

174 animals in experimentation. All research activities in the Antarctic was conducted under

175 National Marine Fisheries Service Permit (808-1735), Antarctic Conservation Act Permit

176 (2009-014), and Duke University Institutional Animal Care and Use Committee (A049-112-

177 02).

178

Data collection

180 Field studies were carried out at two geographically distinct summer feeding grounds of

181 humpback whales (*Megaptera novaeangliae*): the Gulf of St Lawrence in Canada and the

182 western side of Antarctic Peninsula. Animal-borne archival tags used in the study were either

183 3MPD3GT loggers (Little Leonardo Co., Tokyo, Japan) or sound and movement recording

184 DTAGs ([49]; Table 1). The 3MPD3GT loggers were programmed to record depth,

185 temperature, flywheel swim speed and 3-axis magnetism at 1Hz, and 3-axis ± 3 g acceleration

186 at 32Hz. The DTAG sampled pressure and a 3-axis ± 2 g acceleration at 50Hz, which was

187 later downsampled to 5Hz. The 3MPD3GT loggers have the ability to measure flow speed

188 using a front mounted impeller (flywheel). To ensure that speed is measured in the direction

189 of travel, 3MPD3GT tags are mounted in hydrodynamic (tear shaped) floats with a single

190 suction cup mounted at the anterior end, and vertically mounted tail fin at the posterior end.

191 The location of fin and suction cup ensure that the force acting on the tag cause the tag

192 housing to swivel on the animal and orient into the direction of flow. DTAGs are attached to

193 the animal with four suction cups. Tagging was conducted from rigid-hull inflatable boats and

194 either a 5 m or an 8 m handheld carbon fibre pole was used to attach the tag.

196   **Table 1. Humpback whale dataset used for analysis.**

Data ID	Date	Location	Duration (h)	Tag type	Age class	Sex	No of 5-s glides	ρ_{tissue} (kg m^{-1})	C_DAm^{-1} (x10^{-6} m^2 kg^{-1})
Mn11_H584_1	21 Jul 2011	GSL	0.2	3MPD3GT	Adult (pregnant)	F	0	N/A	N/A
Mn11_H607_1	22 Jul 2011	GSL	3.4	3MPD3GT	Adult	M	23	1037.0 ± 1.9	12.5 ± 1.4
Mn11_H686	25 Jul 2011	GSL	4.5	3MPD3GT	Adult	F	75	1036.2 ± 1.2	6.5 ± 2.1
Mn11_H761	25 Jul 2011	GSL	5.9	3MPD3GT	Adult	M	44	1029.0 ± 1.8	16.3 ± 6.5
Mn11_H731	26 Jul 2011	GSL	2.7	3MPD3GT	Adult	F	61	1035.4 ± 1.2	12.8 ± 2.0
Mn11_H698	26 Jul 2011	GSL	2	3MPD3GT	Adult	M	61	N/A	NN/A
Mn11_H228	27 Jul 2011	GSL	0.2	3MPD3GT	Adult	F	3	N/A	N/A
Mn11_H584_2	28 Jul 2011	GSL	3.6	3MPD3GT	Adult (pregnant)	F	47	1028.6 ± 0.7	12.2 ± 1.4
Mn11_H707	19 Aug 2011	GSL	1.6	3MPD3GT	Juvenile	M	93	1043.1 ± 1.6	12.4 ± 1.5
Mn11_H755	28 Aug 2011	GSL	2.9	3MPD3GT	Juvenile	M	177	1033.7 ± 0.5	25.5 ± 1.0
Mn11_H607_2	01 Sep 2011	GSL	2.1	3MPD3GT	Adult	M	29	1031.2 ± 2.3	15.0 ± 9.6
Mn11_H002	04 Sep 2011	GSL	5.8	3MPD3GT	Adult (pregnant)	F	187	1026.5 ± 0.5	6.3 ± 2.8
Mn11_H405	18 Sep 2011	GSL	2.7	3MPD3GT	Adult	M	74	1034.2 ± 0.9	13.1 ± 1.1
Mn11_H489	19 Sep 2011	GSL	0.1	3MPD3GT	Adult	F	0	N/A	N/A
Mn09_121	01 May 2009	A	6.4	Dtag	Adult	U	7	N/A	N/A
Mn09_122	02 May 2009	A	4.2	Dtag	Adult	U	5	N/A	N/A
Mn09_127a	07 May 2009	A	24.2	Dtag	Adult	U	290	1028.4 ± 0.1	11.7 ± 0.2
Mn09_127b	07 May 2009	A	6.5	Dtag	Adult	U	15	N/A	N/A
Mn09_128	08 May 2009	A	2.4	Dtag	Adult	U	11	N/A	N/A
Mn09_136	16 May 2009	A	22.5	Dtag	Adult	U	704	1028.7 ± 0.03	11.2 ± 0.2
Mn09_140	20 May 2009	A	22.3	Dtag	Adult	U	500	1029.8 ± 0.04	9.8 ± 0.2
Mn09_148	28 May 2009	A	25.5	Dtag	Adult	U	30	1026.9 ± 0.7	10.1 ± 2.1
Mn09_151	29 May 2009	A	3.1	Dtag	Juvenile	F	5	N/A	N/A
Mn09_152	01 Jun 2009	A	22.4	Dtag	Adult	U	230	1036.3 ± 0.4	10.5 ± 1.3
Mn10_133	13 May 2010	A	22.8	Dtag	Adult	F	86	1028.6 ± 0.3	6.6 ± 2.4
Mn10_139a	19 May 2010	A	22.2	Dtag	Calf of Mn10_139b	F	118	1040.8 ± 0.5	14.7 ± 0.9
Mn10_139b	19 May 2010	A	23.7	Dtag	Adult	F	457	1029.4 ± 0.1	17.4 ± 1.5
Mn10_143	23 May 2010	A	23.3	Dtag	Unknown	U	77	1026.4 ± 0.3	22.3 ± 3.1

10

Mn10_144	24 May 2010	A	19.9	Dtag	Adult	M	47	1031.1 ± 0.9	6.0 ± 3.5
Mn10_146	26 May 2010	A	20.2	Dtag	Adult	F	419	1029.7 ± 0.1	11.6 ± 0.1
Mn10_151	31 May 2010	A	25	Dtag	Juvenile	F	352	1035.3 ± 0.2	14.0 ± 0.5
Mn10_155a	04 Jun 2010	A	24.2	Dtag	Adult	F	391	1027.6 ± 0.1	14.1 ± 0.3
Mn10_155b	04 Jun 2010	A	22	Dtag	Calf of Mn10_155a	F	67	1025.2 ± 0.4	12.8 ± 1.9

197 GSL and A in the Location column indicate Gulf of St. Lawrence and Antarctica, respectively. Individual-specific estimates of tissue density

198 (ρ_{tissue}) and the combined drag term (C_DAm^{-1}) obtained from the lowest DIC model are presented as mean ± 95% credible interval. Data was not

199 used for the Bayesian estimation when number of 5-s glides was < 20. Dataset shaded with grey were not used for the Bayesian estimation due to

200 insufficient number of 5-s glides in the dataset.

201

Analysis of tag data

Pressure data recorded by archival tags were converted to absolute values of hydrostatic pressure using calibration values and converted to meters. A dive was defined as any submergence to a depth of > 10 m. Dives were broken into descent, bottom and ascent phases based on changes in pitch following Miller *et al.* [38]. As tags were attached to whales at random orientations, the 3-axis acceleration data recorded by the tags was converted to a whale-centred, whale fixed reference frame (whale-frame) using established methods [38, 49]. The accelerometers recorded both specific (e.g. stroking) and gravity-based accelerations (i.e. changes in response to posture change). Under the assumption that changes in the posture of the tagged whale occurred at lower frequency than changes in accelerations resulting from body motions such as thrust, a frequency-based filter (low-pass finite impulse response filters with tag-specific thresholds set at 0.12 – 0.15 Hz) was applied to the entire acceleration time-series to separate these two components. Then, pitch and roll angles of the whales were calculated from the low-frequency component of accelerations [37, 39, 50], while the high-frequency component was used to identify stroking versus gliding periods. For 3MPD3GT dataset, stroking was identified when oscillation on the high-frequency component of surge accelerations indicating fluke beats exceeded a threshold that was set for each deployment ($0.1 – 0.2$ m s^{-2}). Speed sensor data was visually inspected to confirm the presence of stroke-derived acceleration. For DTAG dataset, stroking was detected using high-frequency accelerations at both surge and dorso-ventral axis with thresholds set for each deployment and each axis ($0.1 – 0.2$ m s^{-2}). Gliding periods were automatically detected as the period when the tagged animals did not stroke.

The speed sensor of the 3MPD3GT logger recorded swim speed as the rotation of an external impeller mounted on the anterior end of the logger, which correlates linearly with the speed of

227   water flow passing through the impeller. The rotation rate (number of rotations per second)

228   was converted to speed (m s^{-1}) using a calibration line obtained in-situ for each deployment

229   [37]. The calibration line was obtained from a linear regression of rotation rate against swim

230   speed that was calculated from vertical depth change divided by sine of the pitch at 5 s

231   intervals when absolute mean sine of pitch was greater than 0.7 - 0.9. For the DTAG data,

232   speed during glides was estimated using the rate of change of depth divided by the sine of

233   pitch [38].

234

235   Data during glides were extracted in 5 s duration segments [15]. Glides shorter than 5 s were

236   excluded from the analysis and glides longer than 5 s were broken into 5 s sub-glides. For

237   each 5 s sub-glide, mean depth (d), speed (v) and pitch angle (p) were calculated. Acceleration

238   (a) was measured by regressing speed versus time over each 5-second interval (Fig. S1). The

239   variance of the acceleration measurement during each 5 s sub-glide was quantified as the root

240   mean square of residuals from the fitted regression line. Seawater density (ρ_{sw}) for each sub-

241   glide was calculated from a CTD cast that was made close in time and location to each tagged

242   whale. In this analysis, we only used stable glides (circular variance of roll < 0.1) that were at

243   steep pitch angle (absolute pitch > 30°) to enable robust estimates of speed for DTAG records.

244   In addition, any glides associated with lunge feeding were excluded from the analysis because

245   body form and kinematics of whales drastically change during this feeding behaviour [51].

246   Lunge feeding events were detected as peaks in jerk (i.e. differential of acceleration) for

247   DTAG records [52]. For 3MPD3GT records with speed data, a lunge was detected as peak in

248   speed when the speed exceeded the threshold of mean speed plus two standard deviations

249   followed by a rapid deceleration. According to a fine-scale kinematic study of lunge-feeding

250   humpback whales, whales stroke throughout lunges but glide at the end of feeding once the

251   mouth has been closed [52]. To exclude any feeding-related glides, we excluded any glides

252   recorded within 46 s after the lunge from the analysis because it has been reported that

253   humpback whales spend an average of 46 s for filtration and prey handling [52].

254

Hydrodynamic performance model

256   We used the equation presented by Miller *et al*. [15] where acceleration (m s^{-2}) along the

257   swimming path is determined by drag force (the first term) and buoyancy forces derived from

258   body tissue (the second term) and gasses carried by each whale (the third term):

259    $\text{Acceleration} = -\,0.5 \cdot \frac{C_D \cdot A}{m} \cdot \rho_{sw} \cdot v^2 + \left(\frac{\rho_{sw}}{\rho_{tissue}(d)} - 1 \right) \cdot g \cdot \sin(p)$

$$+ \frac{V_{air}}{m} \cdot g \cdot \sin(p) \cdot \frac{\rho_{sw} - \rho_{air} \cdot (1 + 0.1 \cdot d)}{(1 + 0.1 \cdot d)}$$

260   where:

261    $$\rho_{tissue}(d) = \frac{\rho_{tissue}(0)}{1 - r \cdot (1 + 0.1 \cdot d) \cdot 101325 \cdot 10^{-9}}$$

262

263   Here, C_D is the drag coefficient, A is the relevant surface area (m^2), m is the mass of the whale

264   (kg), ρ_{sw} is the density of the surrounding seawater (kg m^{-3}), v is swim speed (m s^{-1}), ρ_{tissue} is

265   the density of the non-gas component of the whale body (kg m^{-3}), g is acceleration due to

266   gravity (9.8 m s^{-2}), p is animal pitch (radians), V_{air} is the volume of air at the surface (m^3), ρ_{air}

267   is the density of air (kg m^{-3}), d is glide depth (m), and r is compressibility for animal tissue

268   (i.e., the fractional change in volume per unit increase in pressure). The value 101325

269   converts pressure in atmospheres to pressure in Pascals, so that the units of body tissue

270   compressibility are proportion per Pascal x 10^{-9}.

271

272   The first additive term of the equation represents the effect of drag on the forward motion of

273   the whale during a glide, which is primarily a function of speed itself. $C_D A m^{-1}$ is the unknown

274   term that is treated as a single quantity in this approach with units of m^2 kg^{-1}. The second term

275 quantifies the effect of net buoyancy derived from unknown tissue density (ρ_{sw}) on speed

276 during a glide. The third term quantifies the influence of net buoyancy derived from the

277 unknown volume of gas per unit mass carried in the dive ($V_{air}m^{-1}$) on speed during a glide. As

278 gas compartments of whales are compressed during dives, the volume and density of gas

279 carried by the animal are modelled to change with hydrostatic pressure following Boyle's

280 Law. The model also includes the effect of tissue compressibility (r) that was fixed as 0.38 x

281 10^{-9} Pa^{-1} based on the value estimated for northern bottlenose whales [15].

282

Bayesian estimation

284 The unknown parameters in the hydrodynamic glide model (mainly ρ_{tissue}, $V_{air}m^{-1}$ and C_DAm^{-1}

285 ^{1}) were estimated by Bayesian Gibbs sampling with the freely available software JAGS within

286 R (coda, R package v0.17-1 2015, http://cran.r.project.org/web/packages/coda/index.html)

287 and R2jags (R package v0.5-7 2012, https://cran.r-

288 project.org/web/packages/R2jags/index.html) using data extracted for each 5-s sub-glide.

289 Acceleration during glides was measured using a linear regression line of speed versus time.

290 Observation error measured from variance of acceleration for each 5 s was incorporated in the

291 model by treating acceleration as a normal variable with a precision parameter (1/variance)

292 [15]. A small increment (0.001) was added to the standard errors to ensure finite values for

293 the precision parameter. For the Bayesian estimation, a specific prior distribution must be set

294 for each unknown parameter. A non-informative uniform prior from 800 to 1200 kg m^{-3} was

295 set for body tissue density (ρ_{tissue}). An informative prior was set for the combined drag

296 coefficient term (C_DAm^{-1}) based on several sources of information: drag coefficient (C_D) was

297 estimated to be 0.0026 based on the value estimated for a fin whale (*Balaenoptera physalus*)

298 swimming at 4 m s^{-1} [53]. Based on body lengths (L) ranges from 6 to 15 m, body mass (m)

299 was estimated as 20005 kg on average (range 3253 - 48556 kg) using an equation derived for

300   humpback whales: $m = 0.016473L^{2.95}$ x 1000 [54]. Surface area (A) was estimated as 47.4 m^2

301   (range 15.3 – 89.0 m^2) using a prediction equation obtained from bottlenose dolphins

302   (*Tursiops truncatus*): A = $0.08m^{0.65}$ [55]. Thus, an expected value for the combined drag term

303   (C_DAm^{-1}) would be 7 x 10^{-6} m^2 kg^{-1}, with a range from 5 x 10^{-6} m^2 kg^{-1} for large whales to 12

304   x 10^{-6} m^2 kg^{-1} for small whales. In order to capture uncertainty around this expected value, we

305   specify the prior to be a normal distribution with a mean of 7 x 10^{-6} m^2 kg^{-1} and standard

306   deviation of 2 x 10^{-6} m^2 kg^{-1} that was truncated at 1 x 10^{-6} m^2 kg^{-1} and 20 x 10^{-6} m^2 kg^{-1}. For

307   diving gas volume ($V_{air}m^{-1}$), a uniform prior from 5 to 80 ml kg^{-1} was set based on the total

308   lung capacity (65 – 72 ml kg^{-1}) estimated for 6 to 15 m long whales using an equation derived

309   from various marine mammals: total lung capacity = $0.10m^{0.96}$ x 1000 [56].

310

311   Following Miller et al. [15], we explored variability of unknown tissue density, combined

312   drag term and diving gas volume by evaluating a total of 12 model structures. We fitted a

313   model in which the quantity of the unknown parameters ρ_{tissue}, $V_{air}m^{-1}$ and C_DAm^{-1} remained

314   constant across the tags and dives (global estimates). We also fitted hierarchical models in

315   which the individual-specific estimates of tissue density and/or drag term, and the dive-

316   specific estimates for diving gas volume are sampled from each global (i.e. individual-average

317   or dive-average) distribution that was estimated for each parameter. See the JAGS script in

318   the appendix of Miller et al. [15] for the detailed structure of the hierarchical model. All

319   models were sampled in three independent chains, with 24,000 iterations each. The first

320   12,000 samples were discarded for burn-in, and the remaining posterior samples were

321   downsampled by a factor of 36 to remove any serial correlation in the samples. We report the

322   mean and 95% percentile, hereafter termed posterior mean and credible interval (CI), of the

323   posterior samples as the best estimates of the parameter value and its uncertainty. The 95%

324   credible interval is the Bayesian analogue for the more traditional (frequentist) confidence

325   interval, and defines the range of values within which the true parameter value lies with 95%

326   probability, given the observed data. Convergence was assessed for each parameter, using

327   trace history and Brooks-Gelman-Rubin diagnostic plots [57]. The best model was selected

328   based on the deviance information criterion (DIC), with a lower value indicating a better

329   model fit relative to model complexity.

330

331   Results

332   A total of 33 tag datasets were analysed (Table 1). In the Gulf of St Lawrence, archival tags

333   were deployed on 12 whales in the Jacques-Cartier Passage and adjacent waters between July

334   and September 2011. All tagged whales were part of a long-term photo-identification study

335   that has been carried out at the study site since 1984 [58]. Photographic and field observations

336   of behaviour and known associates suggest that at least two adult females (H002 and H584_2)

337   were pregnant when the tag data were collected. Pregnancy of H002 was also confirmed by

338   hormonal analysis of blow samples and blubber samples. One adult male (H607) was tagged

339   twice at the beginning of the feeding season (July 22, 2011) and later the same season

340   (September 1, 2011). At the Antarctic field-site, 19 whales were tagged over the course of two

341   field seasons that ran between May and June in both 2009 and 2010. Antarctic animals were

342   tagged in Wilhelmina and Andvord Bays along the WAP and inshore waters of the Gerlache

343   Strait. Two pairs of tagged whales were found to be mother-and-calf pairs based on visual

344   observation from the tag boat and biopsy samples (Table 1).The whales conducted dives to a

345   maximum depth of 388.3 m. Mean swim speed throughout dives was 1.5 ± 0.4 m s^{-1} ($\pm$ SD,

346   Table 2). Gliding was observed both during descent and ascent phases although the

347   percentage of time spent gliding varied among whales ranging over $1.5 - 45.2\%$ and $2.8 -$

348   60.0% during descent and ascent phases, respectively. Pitch angles during descent and ascent

349   phases were $-39.8 \pm 20.6°$ and $30.6 \pm 22.4°$ on average, respectively (Table 2). From the

350 whole dataset, we extracted a total of 18546 5-s sub-glides that were not associated with a

351 lunge. However, 73.7% of these glides were filtered out due to shallow pitch angle (< 30°)

352 and 0.1% due to high variability in roll (circular variance of roll > 0.9). In addition, 1.4% of

353 glides were removed due to lack of speed and/or acceleration data throughout the 5-s glides.

354 As a result, 24.7% of the total 5-s sub-glides met the criteria for the use of hydrodynamic

355 glide model. The number of 5-s sub-glides that could be used for the hydrodynamic glide

356 model was positively correlated with the duration of tag dataset (Spearman's rho = 0.633, p <

357 0.001; Fig. 1a) although the number of useable glides also varied depending on the behaviour

358 of the tagged whales (foraging, resting, etc.). Eight tag datasets were excluded from the

359 Bayesian estimation of tissue density because of insufficient sample size (<20 sub-glides in

360 each dataset; Table 1). Data of Mn11_H698 was also excluded because an in-situ calibration

361 of the speed sensor was not applicable for this deployment.

362
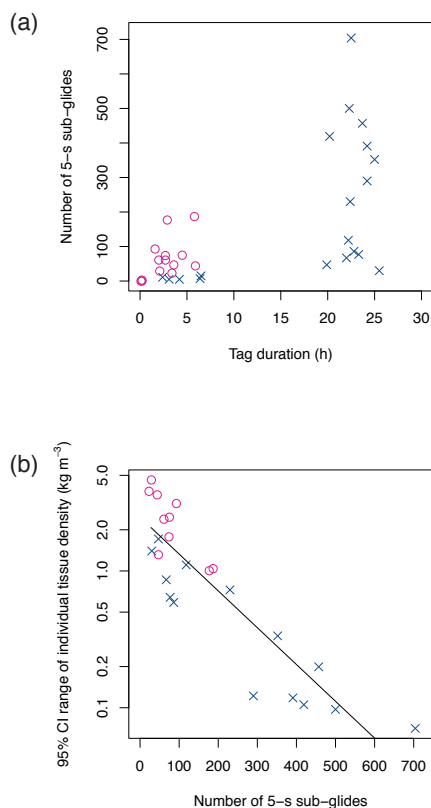
363   **Fig. 1 The number of 5-s sub-glides in relation to tag duration and 95% CI range.**

364   Number of 5-s sub-glides that could be used for the hydrodynamic glide model in relation to

365   tag duration (a) and the range of 95% credible interval for tissue density estimates (b).

366   Magenta circles and blue crosses indicate data from Gulf of St Lawrence and Antarctica,

367   respectively. A solid line shows a regression line: $\log(y) = -0.0062x + 0.90$.

368

369 **Table 2. Summary of dive statistics**

Data ID	N	*Dives* Duration (s)	Depth (m)	Speed (m s⁻¹)	*Descent phase* Duration (s)	Pitch (°)	% time gliding	*Ascent phase* Duration (s)	Pitch (°)	% time gliding
Mn11_H584_1	0	N/A	N/A	N/A	N/A	N/A	N/A	N/A	N/A	N/A
Mn11_H607_1	68	133.1 ± 70.6	45.1 ± 14.4	2.1 ± 0.3	50.8 ± 24.6	-26.0 ± 10.7	7.7 ± 14.4	42.4 ± 20.7	28.8 ± 8.7	6.0 ± 11.3
Mn11_H686	32	204.7 ± 105.8	56.7 ± 60.7	1.3 ± 0.4	63.6 ± 47.7	-18.1 ± 13.5	14.5 ± 21.0	85.8 ± 46.4	23.9 ± 24.5	8.8 ± 16.6
Mn11_H761	51	158.4 ± 110.1	25.3 ± 35.7	1.0 ± 0.3	37.8 ± 26.8	-23.4 ± 14.2	21.1 ± 29.5	91.7 ± 85.6	19.0 ± 13.0	35.1 ± 33.5
Mn11_H731	33	140.9 ± 81.6	44.3 ± 43.6	1.3 ± 0.4	52.5 ± 37.2	-22.0 ± 17.0	31.1 ± 26.9	67.6 ± 41.5	20.8 ± 10.8	38.1 ± 31.8
Mn11_H698	43	101.1 ± 48.3	32.6 ± 18.5	N/A	25.4 ± 8.9	-28.7 ± 16.8	37.3 ± 28.3	56.9 ± 30.1	20.1 ± 9.5	34.1 ± 26.6
Mn11_H228	4	158.0 ± 85.1	24.9 ± 12.2	1.5 ± 0.5	38.5 ± 7.1	-21.7 ± 11.5	42.5 ± 31.4	99.0 ± 80.4	13.0 ± 1.8	60.0 ± 41.4
Mn11_H584_2	32	256.4 ± 153.1	70.0 ± 54.7	2.2 ± 0.6	75.6 ± 41.5	-22.7 ± 16.8	5.5 ± 13.9	96.2 ± 73.9	19.2 ± 9.8	16.1 ± 26.2
Mn11_H707	17	294.1 ± 162.5	116.4 ± 58.6	2.0 ± 0.3	50.1 ± 26.5	-39.2 ± 19.0	45.2 ± 27.5	70.1 ± 30.6	45.7 ± 26.1	6.1 ± 15.4
Mn11_H755	28	328.0 ± 203.0	73.4 ± 45.9	1.3 ± 0.3	58.7 ± 47.1	-32.1 ± 16.4	37.1 ± 33.5	93.4 ± 66.6	19.8 ± 11.8	41.3 ± 31.2
Mn11_H607_2	13	210.0 ± 107.2	64.2 ± 51.3	1.2 ± 0.3	65.2 ± 36.1	-26.2 ± 19.5	19.9 ± 24.3	95.1 ± 79.1	21.0 ± 12.5	8.3 ± 17.8
Mn11_H002	57	217.0 ± 107.2	51.9 ± 41.6	1.3 ± 0.3	63.8 ± 45.3	-18.8 ± 9.3	24.8 ± 24.0	90.4 ± 67.0	15.7 ± 10.4	39.5 ± 31.0
Mn11_H405	24	333.7 ± 194.1	76.6 ± 44.4	1.9 ± 0.3	70.8 ± 36.3	-25.1 ± 12.0	31.9 ± 21.6	72.3 ± 36.9	25.2 ± 14.5	12.0 ± 11.2
Mn11_H489	0	N/A	N/A	N/A	N/A	N/A	N/A	N/A	N/A	N/A
Mn09_121	16	215.4 ± 79.0	48.9 ± 36.4	1.3 ± 0.2	77.0 ± 25.7	-28.9 ± 11.6	23.4 ± 15.4	126.6 ± 56.9	15.1 ± 7.6	58.4 ± 34.1
Mn09_122	48	138.6 ± 73.5	22.8 ± 14.2	1.3 ± 0.5	1.8 ± 27.6	-13.0 ± 11.2	4.7 ± 6.3	67.5 ± 38.6	14.3 ± 7.4	13.4 ± 14.5
Mn09_127a	134	299.1 ± 216.7	127.5 ± 116.7	1.4 ± 0.4	93.8 ± 69.2	-43.1 ± 20.7	9.4 ± 12.6	111.9 ± 86.8	38.5 ± 19.5	23.4 ± 22.9
Mn09_127b	29	211.9 ± 133.6	76.9 ± 71.3	1.8 ± 0.7	61.0 ± 41.5	-35.6 ± 8.7	13.0 ± 15.3	118.6 ± 68.8	9.1 ± 10.8	56.9 ± 27.7
Mn09_128	21	243.9 ± 133.9	32.0 ± 14.1	1.2 ± 0.3	81.1 ± 48.6	-27.2 ± 9.6	13.4 ± 18.2	110.8 ± 71.0	10.3 ± 13.6	29.7 ± 27.3
Mn09_136	101	459.3 ± 136.7	180.8 ± 75.9	1.2 ± 0.2	129.8 ± 51.7	-61.6 ± 15.2	17.0 ± 14.5	159.3 ± 56.3	55.7 ± 20.4	36.8 ± 15.8
Mn09_140	141	357.2 ± 181.2	68.8 ± 72.4	1.4 ± 0.4	89.8 ± 56.9	-23.3 ± 14.1	28.5 ± 20.4	99.2 ± 81.1	20.3 ± 11.6	42.3 ± 25.9
Mn09_148	308	127.4 ± 102.9	40.3 ± 34.9	1.6 ± 0.3	40.2 ± 26.9	-37.1 ± 17.3	5.9 ± 10.7	40.3 ± 31.1	29.7 ± 15.3	14.5 ± 22.5
Mn09_151	18	56.6 ± 29.5	175.9 ± 101.6	1.2 ± 0.6	56.6 ± 29.5	-24.0 ± 7.8	37.0 ± 27.0	97.9 ± 71.8	12.3 ± 10.3	43.5 ± 32.2
Mn09_152	326	118.1 ± 111.5	34.9 ± 30.4	1.3 ± 0.3	39.4 ± 34.1	-48.0 ± 17.6	12.5 ± 19.7	34.6 ± 31.6	29.6 ± 12.7	5.3 ± 12.4
Mn10_133	185	217.0 ± 99.5	76.1 ± 41.7	1.6 ± 0.3	72.2 ± 35.1	-40.0 ± 15.2	1.5 ± 4.6	73.0 ± 42.1	32.9 ± 13.2	10.6 ± 13.6
Mn10_139a	288	170.5 ± 112.3	58.7 ± 38.3	1.5 ± 0.2	36.6 ± 28.4	-53.7 ± 18.1	8.6 ± 17.2	56.1 ± 47.7	44.2 ± 15.0	8.5 ± 15.0
Mn10_139b	285	172.1 ± 100.3	45.8 ± 39.3	1.2 ± 0.3	58.6 ± 35.0	-33.0 ± 15.0	7.0 ± 13.5	70.5 ± 53.2	25.5 ± 14.5	22.3 ± 27.1

20

Mn10_143	286	173.1 ± 107.2	49.5 ± 43.8	1.4 ± 0.5	-54.3 ± 30.1	-32.6 ± 15.3	2.9 ± 7.1	62.4 ± 47.3	25.7 ± 13.6	11.7 ± 18.2
Mn10_144	342	140.8 ± 70.9	52.5 ± 26.1	1.6 ± 0.3	33.2 ± 14.9	-55.9 ± 19.3	4.7 ± 8.6	41.3 ± 24.2	41.0 ± 14.6	2.8 ± 9.1
Mn10_146	88	469.5 ± 147.6	192.5 ± 102.8	1.5 ± 0.3	119.1 ± 47.6	-56.6 ± 22.6	28.4 ± 9.7	143.0 ± 60.8	45.1 ± 26.1	43.6 ± 18.1
Mn10_151	265	191.1 ± 103.7	56.8 ± 41.2	1.4 ± 0.4	53.2 ± 26.6	-44.2 ± 22.4	37.9 ± 31.6	68.8 ± 38.0	29.8 ± 17.7	36.5 ± 33.1
Mn10_155a	153	288.1 ± 179.9	119.3 ± 122.1	1.4 ± 0.4	96.1 ± 73.3	-44.0 ± 21.1	7.9 ± 9.8	96.4 ± 69.6	29.3 ± 27.6	32.6 ± 26.3
Mn10_155b	246	184.2 ± 151.5	58.0 ± 77.1	1.6 ± 0.5	63.9 ± 64.3	-28.5 ± 10.8	5.0 ± 9.3	46.5 ± 43.8	23.1 ± 13.6	8.1 ± 12.4
ALL	*3682*	*199.7 ± 150.1*	*64.0 ± 67.2*	*1.5 ± 0.4*	*58.6 ± 46.8*	*-39.8 ± 20.6*	*12.6 ± 20.0*	*68.1 ± 57.8*	*30.6 ± 22.4*	*18.8 ± 25.1*

370   Mean ± standard deviation were shown. Dataset shaded with grey were not used for the Bayesian estimation due to insufficient number of 5-s

371   glides in the dataset.

372

373   Twenty-four of the 33 tag datasets (10 from the Gulf of St Lawrence and 14 from Antarctica)

374   were used to estimate tissue density and the other unknown parameters. Of the 12 Bayesian

375   models, the model with the lowest DIC indicated global plus individual variation in tissue

376   density and drag terms, and global plus dive-by-dive variability in diving lung volume (Table

377   3). The difference in DIC from the next-best model was 1657.5 units.

378

Table 3. Model parameter values.

| Model fit	Model structure			Global parameter estimates					
DIC	ρ_{tissue}	C_DAm^{-1}	V_{air}	ρ_{tissue}.g	ρ_{tissue}.var	C_DAm^{-1}.g	C_DAm^{-1}.var	V_{air}.g	V_{air}.var
28301.1	I	I	D	1031.6 (2.1)	26.5 (17.2)	11.8 (1.6)	23.2 (16.4)	27.7 (1.1)	236.5 (33.4)
29958.6	I	G	D	1031.3 (2.1)	25.4 (16.2)	11.6 (0.1)		26.5 (1.1)	199.8 (25.6)
53399.8	G	I	D	1029.4 (0.02)		7.9 (3.2)	349.8 (369.6)	21.0 (1.4)	353.2 (57.2)
86274.2	G	G	D	1029.7 (0.02)		8.3 (0.1)		20.7 (1.5)	502.8 (89.2)
106380.0	I	I	I	1030.3 (1.8)	19.8 (11.8)	8.5 (2.5)	103.8 (86.0)	25.7 (7.2)	305.2 (288.2)
113957.5	I	G	I	1030.1(1.7)	17.3 (11.1)	9.3 (0.1)		23.5 (5.8)	193.1 (170.0)
120768.9	I	I	G	1029.0 (1.1)	6.5 (4.1)	6.7 (1.8)	39.7 (26.7)	15.6 (0.1)	
125832.6	G	I	I	1029.0 (0.02)		7.3 (3.2)	215.5 (240.8)	19.3 (6.5)	227.8 (238.8)
130603.2	I	G	G	1029.2 (1.13)	7.4 (4.5)	7.9 (0.1)		15.9 (0.1)	
159607.6	G	G	I	1029.2 (0.01)		6.9 (0.1)		24.5 (17.0)	1515.3 (2882.9)
264515.3	G	I	G	1028.1 (0.01)		6.7 (3.5)	1930.7 (7548.2)	8.6 (0.1)	
309390.4	G	G	G	1028.0 (0.01)		1.3 (0.04)		7.2 (0.1)	

Model structure refers to the allowed variation in the model for the unknown terms, with G referring to global (i.e. individual-average) parameter only, I referring to individual specific estimates included, and D referring to dive-by-dive variation included. The column head refer to ρ_{tissue} as tissue density (kg m^{-3}); C_DAm^{-1} as combined drag term (m^2 kg^{-1}); V_{air} as volume of air (ml kg^{-1}). Data are presented with ±95% CI in parentheses.

For global parameter estimates, .g refers to the global parameter and .var refers to individual or dive-by-dive variance.

385 The global body tissue density was estimated with a posterior 95% credible interval (CI) of

386 1029.5 – 1033.6 kg m^{-3} (mean = 1031.6 kg m^{-3}). Individual posterior mean values ranged

387 from 1025.2 to 1043.1 with ±95% CI of 0.04 – 2.3 kg m^{-3}. The 95% CI range for individual

388 tissue density estimates decreased with increasing number of 5-s sub-glides in the dataset

389 (Fig. 1b). There was no significant relationship between the 95% CI range and the average

390 depth at which the sub-glides occurred (Spearman's rank test, p = 0.22); depth of glides

391 ranged from 5.1 to 343.2 m with individual mean ranging 25.2 ± 10.8 to 97.3 ± 55.4 m. There

392 was a tendency for the 95% CI ranges to be smaller for the whales tagged in Antarctica using

393 DTAGs (0.6 ± 0.66 kg m^{-3}) than in the Gulf of St Lawrence using 3MPD3GTs (2.4 ± 1.11 kg

394 m^{-3}). It is possible that different sampling frequencies and resolution of sensors as well as

395 speed determination methods (measured/estimated) of 3MPD3GTs and DTAGs might

396 influence the precision of tissue density estimates. Yet, the effect of the two different archival

397 tag models could not be fully addressed due to the differences in location itself and longer

398 data duration for the Antarctic DTAG dataset (22.9 ± 1.6 h) compared to the Gulf of St

399 Lawrence 3MPD3GT dataset (3.5 ± 1.5 h; Table 1).

400

401 Whales in the Gulf of St Lawrence had relatively higher tissue density (median = 1034.0 kg

402 m^{-3}, range = 1026.5 – 1043.1 kg m^{-3}) than Antarctic whales (median = 1029.0 kg m^{-3}, range =

403 1025.2 – 1040.8 kg m^{-3}) although there was high inter-individual variation within each

404 feeding population (Fig. 2). The posterior mean tissue density of the male Mn11_H607 that

405 was tagged twice in July and September 2011 in the Gulf of St Lawrence decreased by 5.8 kg

406 m^{-3} in 40 days (Table 1). Tissue densities of two pregnant females were estimated as the

407 lowest (1026.5 ± 0.5 kg m^{-3} for Mn11_H002) and the second lowest (1028.6 ± 0.7 kg m^{-3} for

408 Mn11_H584_2) among the whales from the Gulf of St Lawrence (Table 1). There was a

409 significant negative correlation between relative tissue density to seawater and percent time

410 spent gliding during ascent vs decent phases of non-feeding dives (Spearman's rho = -0.72, p

411 <0.001; Fig. 3).
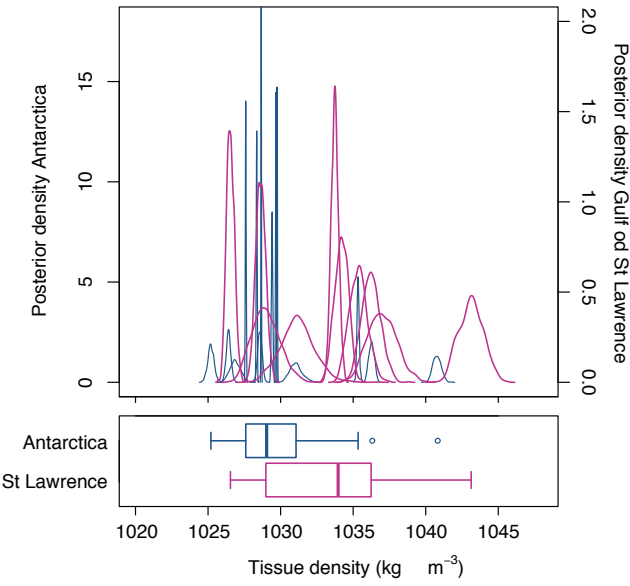
412

413 **Fig. 2 Tissue density estimates from the best model with the lowest DIC.** The top panel

414 shows posterior distribution of individual body tissue density for each tag deployment. Blue

415 and magenta lines indicate whales from Antarctica and the Gulf of St Lawrence, respectively.

416 Box plots in the bottom panel show median and interquartile range of tissue density estimates

417 from each location.

418
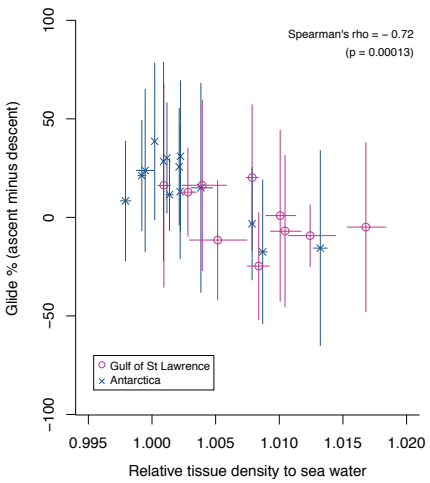
419   **Fig. 3 Relationship between gliding patterns and relative tissue density.** The y-axis

420   indicates differences in the percentage of time spent gliding during ascent and descent phases

421   of non-feeding dives by each whale. Vertical and horizontal error bars show standard

422   deviation and 95% credible interval range, respectively. A relative tissue density of >1

423   indicates that tissue density was denser than surrounding seawater.

424

425

426   The posterior mean of the global drag term was $11.8 \times 10^{-6} \pm 1.6 \times 10^{-6}$ m^2 kg^{-1} ($\pm$ 95% CI).

427   The posterior mean was higher and the distribution had little overlap with the prior

428   distribution that had a mean of 7.0×10^{-6} m^2 kg^{-1} (Fig. 4). The posterior means of individual

429   drag term values ranged from 6.0×10^{-6} to 25.5×10^{-6} m^2 kg^{-1}, but most of them were near

430   12.5×10^{-6} m^2 kg^{-1} (Table 1). The posterior mean of global diving gas volume was 27.7 ± 1.1

431   ml kg^{-1} ($\pm$95% CI).

432

433   The best-fitting model with the lowest DIC evaluated dive-by-dive variation in diving gas

434   volume. The dive-by-dive estimates of diving gas volume ranged from 0.03 to 129.2 ml kg^{-1},

435   but 90% of the estimates were within 9.2 – 53.5 ml kg^{-1}. Diving gas volume was estimated

436   slightly higher for feeding dives with more than 1 lunge (median = 26.3 ml kg^{-1}, range = 2.6 –

437   110.8 ml kg^{-1}) than other dives (median = 21.3 ml kg^{-1}, range = 0.8 – 97.5 ml kg^{-1}; Wilcoxon

438   rank sum test, p =0.021). Weak correlations between diving gas volume and dive depth were

439   observed for both feeding (Spearman's rho = 0.09, p = 0.036, N = 515) and non-feeding dives

440   (Spearman's rho = 0.21, p < 0.001, N = 252). However, no apparent relationships between

441   diving gas volume and dive duration were observed for feeding (Spearman's rho = 0.02, p =

442   0.58, N = 515) or non-feeding dives (Spearman's rho = 0.05, p = 0.45, N = 252).
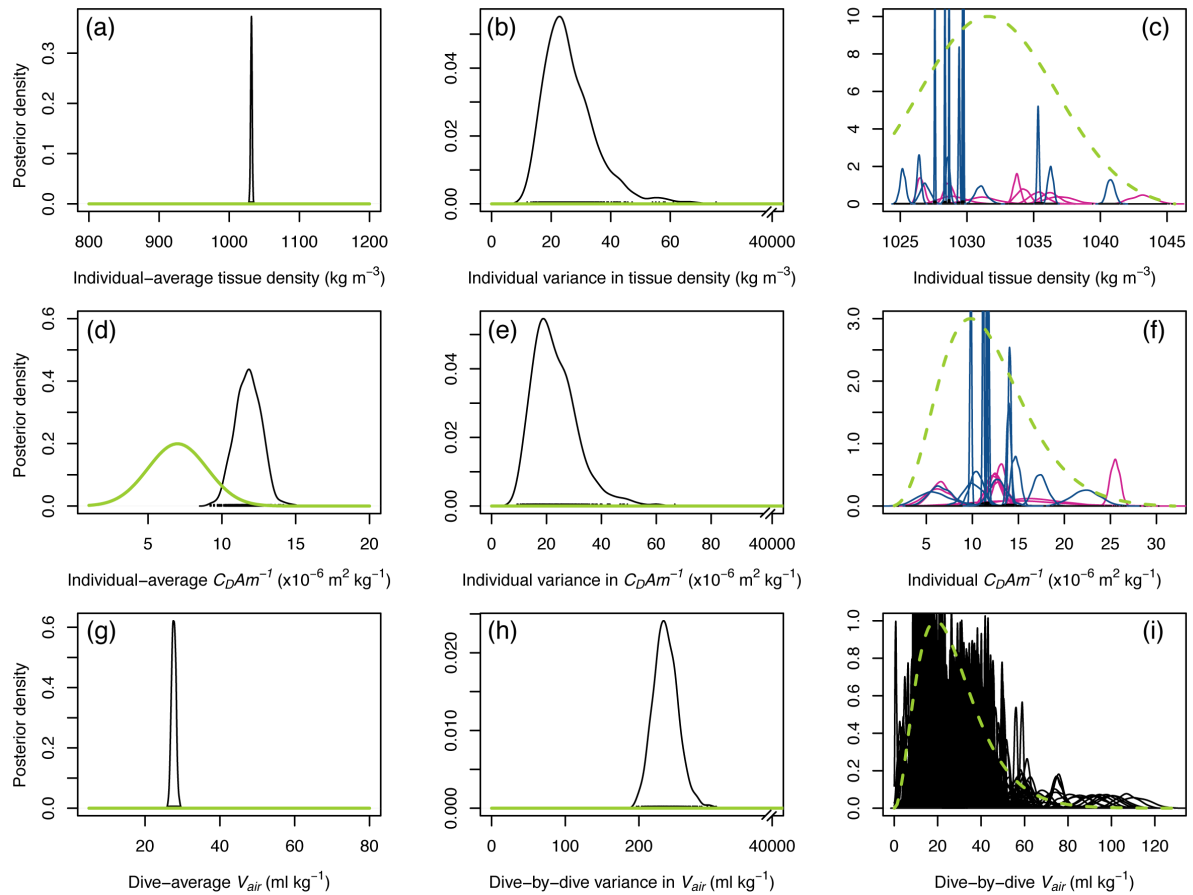
443

Fig. 4 Prior and posterior distributions from the model with lowest DIC (Table 3). Prior

and posterior distributions of tissue density (a, b, c), drag term (d, e, f) and diving gas volume

(g, h, i) are shown in each panel. Solid green and black lines indicate the prior and posterior

distributions, respectively. Dashed green lines show the estimated global distribution that can

be interpreted as the population distribution for that parameter. The left and middle panels

show global parameters (a, b, d, e, g, h) and the right parameters show individual and dive-

specific parameters.

Discussion

To date, the hydrodynamic glide model has been used to estimate tissue density of deep

diving marine mammals such as elephant seals, sperm whales, northern bottlenose whales and

27

456   long-finned pilot whales [15, 34, 38, 47]. In this study, we successfully applied this method to

457   substantially shallower-diving humpback whales to estimate tissue density from two

458   geographically distinct feeding populations. To examine the variability of the unknown

459   parameters (tissue density, drag and diving gas volume), we fitted 12 models with different

460   model structures. The best model included individual variation in tissue density and drag,

461   supporting our expectation that each whale had different tissue density. The best-fitting model

462   also included dive-by-dive variation in diving gas volume. Although there was no apparent

463   overall relationship between diving gas volume and dive duration, it is possible that whales

464   change the amount of inhaled air before dives depending on their activity [15]. The gliding

465   patterns of whales correlated with their estimated tissue density, with denser whales spending

466   relatively more time gliding during descent and less-dense whales spending more timing

467   gliding during ascent phases (Fig. 3). The significant correlation of tissue density and gliding

468   patterns provides a degree of validation that the tissue density estimates, or at least their

469   relative values, were accurate.

470

471   **Drag term estimates**

472   The drag coefficient is one of the key parameters to estimate tissue density using the

473   hydrodynamic glide model. Following Miller et al. [15], the combined drag term ($C_D A m^{-1}$)

474   was estimated using a relatively narrow Gaussian prior that was determined based on

475   auxiliary published data in order to improve the precision of tissue density estimates.

476   However, the global (individual-average) estimate of the drag term in the best-fitting model

477   (11.8×10^{-6} m^2 kg^{-1}) did not concentrate within the distribution of the prior (7.0×10^{-6} m^2 kg^{-1}

478   ^{1}).

479

480 As in previous studies [15, 34, 38], we neglected any specific effect of lift, although lift-

481 related induced drag may not be negligible in the case of humpback whales due to their large

482 pectoral flippers [48] and propensity to glide at shallow angles. It is possible that the influence

483 of induced drag due to lift generation may explain the mismatch of the prior expectation of

484 the combined drag term and its posterior estimate from the data. Adding the induced drag to

485 the hydrodynamic glide model, the drag part of the equation can be expressed as

$$-0.5\rho_{sw}\frac{C_D A}{m}v^2 - 0.5\rho_{sw}\frac{A_{Flipper}}{\pi AR}\frac{C_L^2}{m}v^2$$

486 where $A_{Flipper}$ is flipper surface area (m^2), AR is flipper aspect ratio and C_L is the lift

487 coefficient [59]. Because both the parasite drag and the induced drag are a function of speed-

488 squared, the equation can be rewritten as

$$-0.5\rho_{sw}\left(\frac{C_D \cdot A}{m} + \frac{A_{Flipper}}{\pi \cdot AR}\cdot\frac{C_L^2}{m}\right)v^2$$

489 Thus, the structure of the equation is unchanged just with the addition of induced drag to that

490 of the parasite drag term $C_D A m^{-1}$.

491

492 We suggest that the model estimated higher global $C_D A m^{-1}$ values due to the effect of induced

493 drag by assuming that the model estimated the combined term in parenthesis, instead of the

494 parasite drag term ($C_D A m^{-1}$) alone. The lift coefficient of a humpback whale flipper is

495 estimated as $0 - 0.9$ through wind tunnel measurements [60]. Based upon literature values for

496 the surface area ($A_{Flipper}$, 12.20 m^2) and the aspect ratio (AR, 5.67) of a humpback whale

497 flipper [48], $A_{Flipper}C_L^2/(\pi AR m)$ is estimated as $0 - 22$ x 10^{-5} for a 12-m long whale. Adding

498 this value to 7 x 10^{-6} (i.e. mean of the $C_D A m^{-1}$ prior), the combined drag term in the

499 parenthesis is expected to range between 7 x 10^{-6} and 29 x 10^{-6} m^2 kg^{-1} which overlaps with

500 the global drag term estimates in this study (11.8 x 10^{-6} ± 1.6 x 10^{-6} m^2 kg^{-1}, ± 95% CI). This

501   suggests that the mismatch between the prior and $C_D A m^{-1}$ estimates derived from the addition

502   of the induced drag and that lift-related drag forces should not be ignored for this species.

503

504   In comparison with deeper diving marine mammals in previous studies [15, 34], the effect of

505   lift seems particularly important for humpback whales that glide at shallower pitch angles

506   (Table 2) where lift generation increases with correspondingly greater induced drag.

507   Humpback whales have large flipper with a high aspect ratio that can produce lift forces to

508   support their acrobatic movements such as high-speed turning and banking that are associated

509   with feeding [48, 61]. In addition, the scalloped leading edge of their large flippers serves to

510   delay stall angles and increase lift [60, 62]. Recent studies using animal-borne video camera

511   reported that humpback whales also perform lift-generating flipper strokes for propulsion

512   during lunge feeding [63]. In our study, we only used data during stable glides (circular

513   variance of roll < 0.1) to minimize the influence of lift during maneuvering. However, the

514   influence of lift-induced drag is detectable in our dataset possibly because humpback whales

515   likely use their wing-like flippers to produce lift during stable glides at non-vertical pitch

516   angles. Yet, it is noteworthy that our general results about tissue density seem to be robust

517   because the model quantified the combined effect of parasite and induced drag. As a

518   sensitivity analysis, we refitted the model using a non-informative wide range prior for the

519   drag term instead of a narrow Gaussian prior. The resulting global average drag term was 13.1

520   x $10^{-6} \pm 2.4$ x 10^{-6} m^2 kg^{-1} and global average tissue density was 1031.6 ± 2.1 kg m^{-3}, which

521   differed very little from the estimated values with a narrow prior. Similarly, individual tissue

522   density estimates were nearly identical to the result of our original model, supporting the

523   robustness of the tissue density estimates to the prior specification. Thus, the general results

524   about tissue density seem to be robust because the model appears to have estimated a

525   reasonable value for the combined effect of parasite and induced drag.

Body tissue density

527

528   Estimated individual-average (global) body tissue density of humpback whales (1031.6 ± 2.1

529   kg m^{-3}; Table 3) was similar to that of other cetaceans reported to date (1030.0 ± 0.8 kg m^{-3}

530   for *Physeter macrocephalus* [38]; 1031.5 ± 1.0 kg m^{-3} for *Hyperoodon ampullatus* [15]),

531   indicating that non-gas body tissues are typically denser than seawater. However, long-finned

532   pilot whales were estimated to have even denser tissues of 1038.8 ± 1.60 kg m^{-3} [47]. For

533   humpback whales in this study, a large variation was detected in individual-specific body

534   tissue density ranging from 1025.2 to 1043.1 kg m^{-3}, as we expected, because individual

535   tissue density at feeding grounds would change depending on factors such as age, sex,

536   reproductive status, prey availability and the number of days since arrival at the feeding

537   ground [4, 6, 18, 24]. In a study of fin whales conducted using Icelandic whaling data,

538   pregnant females had the highest rate of fattening during the feeding season as they increased

539   their total body energy content by nearly 80% [4]. A similar trend was reported for minke

540   whales (*Balaenoptera acutorostrata*) in Iceland: the blubber volume of pregnant females

541   almost doubled over the feeding season [24]. Using the hydrodynamic glide model, high

542   lipid-stores of two pregnant female humpback whales (Mn11_H002 and Mn11_H584_2) were

543   indicated by low tissue density estimates of 1026.5 kg m^{-3} and 1028.6 kg m^{-3} that were the

544   lowest and the second lowest, respectively, among all of the tagged whales in the Gulf of St

545   Lawrence. A decrease in tissue density over the feeding season due to accumulation of lipid

546   stores was also detected in this study: tissue density of a repeated sampled adult male

547   (Mn11_H607) decreased from 1037.0 to 1031.2 kg m^{-3} in 40 days. Based on extrapolation

548   from elephant seals, the proportion of lipid content (P_{lipid}) corresponding to these tissue

549   densities of Mn11_H607 would be 36.3% and 39.0%, as determined from $\rho_{tissue} =$

550    $\rho_{lipid}P_{lipid} + \rho_{lipid\text{-}free}(1 - P_{lipid})$, where ρ_{lipid} and $\rho_{lipid\text{-}free}$ are 900.7 and 1114.6 kg m^{-3}, respectively

551   [34]. Our results also showed that one of the two calves had low body tissue density of 1025.2

552   kg m^{-3} (Mn10_155b) in agreement with general expectation that calves are more buoyant

553   because they deposit fat during the lactation period [64]. The other calf (Mn10_139a),

554   however, had relatively high tissue density of 1040.8 kg m^{-3} that was supported by its gliding

555   pattern suggestive of negative buoyancy: the whale spent more time gliding during descent

556   (61.3%) than ascent (45.7%) phases of non-feeding dives (Fig. 5d). It is possible that

557   Mn10_139a had a poor body condition, reflecting its mother's poor condition indicated by its

558   relatively high body density (Mn10_139b, 1029.4 kg m^{-3}) compared to the other mother in the

559   study (Mn10_155a, 1027.6 kg m^{-3}).

560   During the feeding season, it is essential for humpback whales to accumulate a sufficient

561   amount of energy for survival, growth and/or reproduction. Previous studies estimated the

562   amount of energy gained by baleen whales over the course of a feeding season via anatomical

563   measurements and chemical analysis of multiple whale carcasses [4, 21]. More recent work

564   has described dynamic foraging patterns of whales throughout the course of the foraging

565   season suggesting that whales alter their feeding behaviour (rates and dive depth)

566   commensurate with changes in the availability of prey [65]. This could lead to non-linear

567   changes in the accumulation of energy, and, combined with body density estimates collected

568   over similar time periods, can offer insights as to the most critical times and locations for

569   whales to regain energy stores and how different life history classes vary. This information is

570   critical to understanding how environmental changes and potential human disturbance can

571   significantly impact individual and population-level health of marine mammals and other
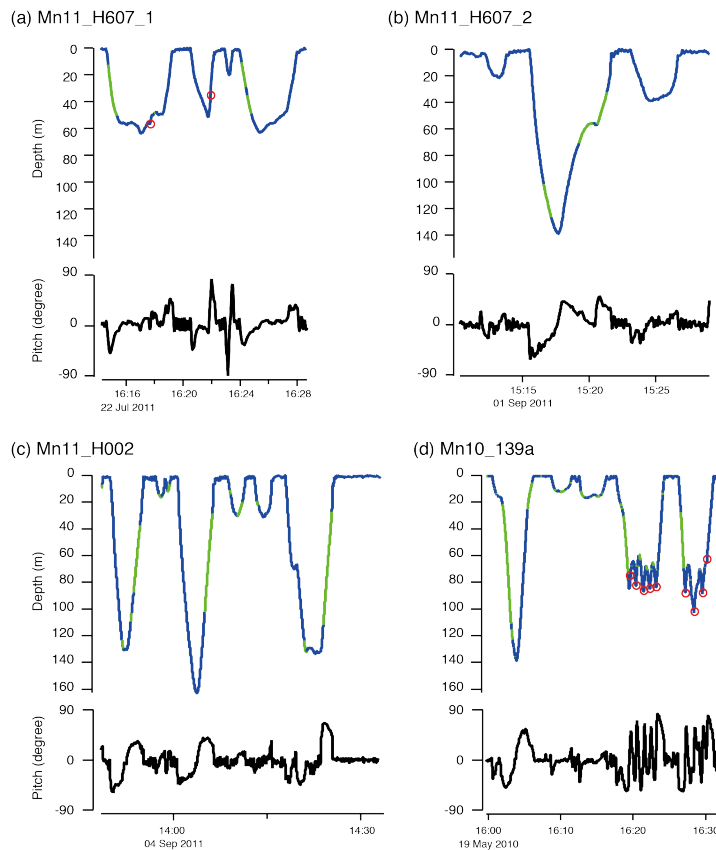
572   animals.

573

Fig. 5 Example data records for dive profile and pitch. Dive profile with gliding and stroking periods are indicated in green and blue, respectively. Red circles indicate feeding events. Examples are taken from an adult male during (a) early feeding season (tissue density = 1037.0 kg m^{-1}) and (b) late feeding season (1031.2 kg m^{-1}), (c) a pregnant female (1026.5 kg m^{-1}) and (d) a calf (1040.8 kg m^{-1}).

Changes in tissue density lead to changes in buoyancy that influence swimming patterns of diving animals given strong selection for them to travel efficiently to and from depth [33, 39]. For example, it is expected that animals with higher density should glide more during descent aided by negative buoyancy whereas less dense positively buoyant animals should employ more glides during ascent. In agreement with the expectation, a negative correlation between tissue density estimates and percent time spent gliding during ascent vs. descent phases of non-feeding dives was observed (Fig. 3), suggesting that the model successfully detected

588 relative differences in individual tissue density. Because there is greater variability in tissue

589 density of humpback whales than deep diving toothed whales [15, 38, 54], the relatively low

590 precision of tissue density estimates obtained here (±95% CI of individual tissue density

591 ranged up to 2.3 in this study whereas to 0.4 in [15]) seem to be sufficient to detect individual

592 and/or temporal variation. Lower precision tissue density estimates may be expected if there

593 is high variability in acceleration that is not accounted for in the model. Therefore, sample

594 size is particularly important to consider for the body density estimation of humpback whales

595 for which induced drag may cause variability in gliding acceleration. The result showed that

596 the number of 5-s sub-glides in each dataset is one of the key factors affecting the range of

597 95% CI for the posterior estimates of individual tissue density. Specifically for humpback

598 whales, >200 sub-glides in each dataset seem to be needed to obtain highly precise estimates

599 with 95% CI range of 1 kg m^{-3} (Fig. 1b).

600

601   In this study, we estimated tissue density of humpback whales at two geographically distinct

602 feeding grounds. Tissue density of whales from Antarctica and Gulf of St Lawrence largely

603 overlapped, but there was a tendency for Antarctic whales to have lower tissue density (Fig.

604 2), indicating that animals in that location at that time had larger lipid reserves than did the

605 animals tagged in Canada. It is possible that the geographic differences reflected different

606 temperature and prey conditions on two feeding grounds. However, as numerous factors can

607 affect individual tissue density, more data, including basic information of individuals such as

608 sex, age class and reproductive status that can be obtained from photo-ID and biopsy studies

609 would be essential to identify factors that cause these geographic differences.

610

611 The methods used in this study closely followed methods published for other deep-diving

612 odontocete species. Some studies used an estimated value of 0.06 for the entrained mass of

613   water m_e which is moved forward along with the body of the animal [38]. Because we did not

614   have specific measurements of animal mass in this study, we also did not include estimates

615   for entrained mass. We also do not expect addition of a constant mass proportion of mass to

616   all estimates would affect their relative values. However, the absolute values obtained in this

617   study could be made more accurate with finer estimates of the length, mass and surface area

618   of each whale as was done using photogrammetry by Miller et al. [38]. We do recommend

619   incorporation of such data when available, and to include estimates of entrained mass to

620   obtain accurate absolute values of tissue body density.

621

Diving gas volume

623   The posterior mean of global (dive-average) diving gas volume was 27.7 ± 1.1 ml kg^{-1} ($\pm95\%$

624   CI). This value is substantially lower than the estimated lung volumes of mysticete fin (29 –

625   61 ml kg^{-1}) and sei (*Balaenoptera borealis*) whales (116 – 151 ml kg^{-1}), whose lung volumes

626   were measured via inflation of excised lungs [66, 67]. This could indicate that: 1) lung

627   volumes of mysticete whales are smaller than estimated from excised lungs in which some

628   amount of air is likely to be trapped [46]. Piscitelli et al. [67] noted that the mass specific

629   volume of sei whales from that study were outliers on a comparative basis relative to smaller

630   cetaceans; 2) humpback whales in this study dove with less than their full lung capacity; or 3)

631   our estimate was incorrect and too low.

632

633   As cetaceans appear to inhale immediately prior to diving, the diving volume of cetaceans is

634   thought to be close to the total lung volume [68]. In fact, the calculated diving lung volume of

635   deep-diving northern bottlenose whales (27 ml kg^{-1}, [15]) was similar to the measured total

636   lung volume of 28 ml kg^{-1} ([69] reviewed in [68]). However, shallower diving species may

637   not always dive with full lungs; for example, the diving lung volume and the total lung

638   volume of bottlenose dolphins are 40-50 ml kg^{-1} [70] and 50-91 ml kg^{-1}, respectively

639   (reviewed by [67]). Differences in lung sizes and thoracic morphology of shallow and deep

640   diving cetaceans have been reported [46]. As the effect of air-derived buoyancy is stronger at

641   shallower depth, it is possible that shallower-diving whales do not always dive with full lung

642   capacity. A large variation in dive-by-dive estimates of diving gas volume found in this study

643   and, albeit weak, the positive relationship between diving gas volume and dive depth would

644   support this hypothesis. While no systematic variation of diving gas volume in relation to dive

645   duration was detected, further detailed analysis of dive-by-dive variation in diving gas volume

646   could provide new insights into their diving physiology.

647

648   Another possible explanation for the low estimate of diving gas volume is that the amount of

649   gas stored in the body might decrease during dives. It has been reported that humpback

650   whales actively exhale underwater in some situations. For example, humpback whales have a

651   diverse repertoire of feeding behaviours, including "bubble feeding" that involves underwater

652   exhalation to form bubble clouds, nets or curtains to corral prey [61, 71]. Bubbling is also

653   observed in non-feeding situations such as play [71] and social interactions [72]. Although

654   apparent bubbling was not detected from acoustic audits of the DTAG datasets in this study, it

655   is possible that some air might passively escape from the body during dives.. If such

656   underwater exhalation and/or passive loss of air occurred, our estimate of diving gas volume

657   would be too low because the majority of the glides used in the analysis were recorded during

658   ascent phases of dives, and thereby the estimate reflects the amount of gas in the body at latter

659   part of dives.

660

661   **Conclusion and future directions**

662   We demonstrated that the hydrodynamic glide model can be used to detect individual and

663   temporal variation in body tissue density of humpback whales, suggesting that it is likely to

664   be broadly applicable across a range of aquatic animals including shallow diving baleen

665   whales. The important next step is validation with other techniques such as visual assessment

666   [28, 29], biopsy sample measurements, and photogrammetric measurements of body width

667   versus length using overhead images [11, 30].

668

669   This study represents a cross-sectional design, in which the tissue densities of multiple

670   animals were measured. Longitudinal tracking of changes in individuals' tissue density as has

671   been done with elephant seals drift dives [5], or repeated measurements as we made for whale

672   Mn11_H607, may be a more powerful approach to determine specific factors that affect the

673   lipid-store body condition of humpback whales. Considering that humpback whales are less

674   difficult to tag such that multiple tagging of the same individual is possible, this tag-based

675   minimally invasive approach may provide an effective tool to monitor body tissue density as a

676   measure of body condition. By integrating life-history data of individuals (e.g. age, sex, size,

677   reproductive status) as well as prey availability at feeding grounds, this approach can be

678   helpful to understand bioenergetics and health of individual whales within increasingly

679   human-altered ecosystems. Ultimately, tracking the tissue density of individual whales using

680   longer duration tags could be a powerful technique to relate their body condition to how they

681   interact with features of their natural environment.

682

683

684   **Acknowledgements**

37

687   to thank to all staffs and volunteers in Mingan Island Cetacean Study for field data collection.

688   We also thank the scientific and technical staff on the Antarctic cruises, particularly those

689   involved with tagging and tag data processing: Alison Stimpert, Ann Allen.

690

691 **References**

692   1.   Heithaus MR, Frid A, Wirsing AJ, Dill LM, Fourqurean JW, Burkholder D, Thomson J,

693   Bejder L. State-dependent risk-taking by green sea turtles mediates top-down effects of

694   tiger shark intimidation in a marine ecosystem. J Anim Ecol. 2007; 76: 837-844.

695   2.   Bêty J, Gauthier G, Giroux J. Body condition, migration, and timing of reproduction in

696   snow geese: a test of the condition-dependent model of optimal clutch size. Am Nat.

697   2003; 162: 110-121.

698   3.   Crossin GT, Phillips RA, Wynne-Edwards KE, Williams TD. Postmigratory body

699   condition and ovarian steroid production predict breeding decisions by female gray-

700   headed albatrosses. Physiol Biochem Zool. 2013; 86: 761-768.

701   4.   Vikingsson GA. Body condition of fin whales during summer off Iceland. Developments

702   in Mar Biol. 1995; 4: 361-369.

703   5.   Biuw M, McConnell B, Bradshaw CJA, Burton H, Fedak MA. Blubber and buoyancy:

704   monitoring the body condition of free-ranging seals using simple dive characteristics. J

705   Exp Biol. 2003; 206: 3405-3423.

706   6.   Williams R, Vikingsson GA, Gislason A, Lockyer C, New L, Thomas L, Hammond PS.

707   Evidence for density-dependent changes in body condition and pregnancy rate of North

708   Atlantic fin whales over four decades of varying environmental conditions. ICES J Mar

709   Sci. 2013; 70: 1273-1280.

710   7.   Christiansen F, Vikingsson GA, Rasmussen MH, Lusseau D. Female body condition

711   affects foetal growth in a capital breeding mysticete. Funct Ecol. 2014; 28: 579 - 588

712 8. Pomeroy PP, Fedak MA, Anderson SS, Rothery P. Consequences of maternal size for

713   reproductive expenditure and pupping success in grey seals at North Rona, Scotland. J

714   Anim Ecol. 1999; 68: 235-253.

715 9. McMahon CR, Burton HR, Bester MN. Weaning mass and the future survival of

716   juvenile southern elephant seals, *Mirounga leonine*, at Macquarie Island. Antarct Sci.

717   2000; 12: 149-153.

718 10. Hall AJ, McConnell BJ, Barker RJ. Factors affecting first-year survival in grey seals and

719   their implications for life history strategy. J Anim Ecol. 2001; 70:138-149.

720 11. Christiansen F, Dujon AM, Sprogis KR, Arnould JPY, Bejder L. Noninvasive unmanned

721   aerial vehicle provides estimates of the energetic cost of reproduction in humpback

722   whales. Ecosphere. 2016; 7: 1 – 18.

723 12. Friedlaender AS, Tyson RB, Stimpert AK, Read AJ, Nowacek DP. Extreme diel

724   variation in the feeding behaviour of humpback whales along the western Antarctic

725   Penninsula during autumn. Mar Ecol Prog Ser. 2014; 494:281-239.

726 13. Friedlaender AS, Johnston DW, Tyson RB, Kaltenberg A, Goldbogen JA, Stimpert AK,

727   Curtice C, Hazen EL, Halpin PN, Read AJ, Nowacek DP. Multiple-stage decisions in a

728   marine central-place forager. P Soc Open Sci. 2016; 3: 160043.

729 14. Stevenson RD, Woods WA Jr. Condition indices for conservation: new uses for evolving

730   tools. Integr Comp Biol. 2006; 46: 1169-1190.

731 15. Miller P, Narazaki T, Isojunno S, Aoki K, Smout S, Sato K. Body density and diving gas

732   volume of the northern bottlenose whale (*Hyperoodon ampullatus*). J Exp Biol. 2016;

733   219: 2458-2468.

734 16. National Research Council (NRC). Approaches to understanding the cumulative effects

735   of stressors on marine mammals. Washington DC: The National Academies Press; 2017.

736   Available from: http://www.nap.edu/23479

737   17. Kasuya T. Overview of cetacean life histories: an essay in their evolution. Dev Mar

738   Biol. 1995; 4: 481-498.

739   18. Lockyer C. Body fat condition in Northeast Atlantic fin whales, *Balaenoptera physalus*,

740   and its relationship with reproduction and food resource. Can. J. Fish. Aquat. Sci. 1986;

741   43:142-147

742   19. Aguilar A, Borrell A. Patterns of lipid content and stratification in the blubber of in

743   whales (*Balaenoptera physalus*). J Mammal. 1990; 71: 544-554.

744   20. Konishi K. Characteristics of blubber distribution and body condition indicators for

745   Antarctic minke whales (*Balaenoptera bonaerensis*). Mammal Study. 2006; 31: 15-22.

746   21. Lockyer C. Evaluation of the role of fat reserves in relation to the ecology of North

747   Atlantic fin and sei whales. In: Huntley AC, Costa DP, Worthy GAJ, Castellini MA,

748   editors. Approaches to Marine Mammal Energetics. Special Publication No 1. Lawrence:

749   Society for Marine Mammalogy; 1987. pp. 183-203.

750   22. Næss A, Haug T, Nilssen EM. Seasonal variation in body condition and muscular lipid

751   contents in northeast Atlantic Mike whale *Balaenoptera acutorostrata*. Sarsia 1998; 83:

752   211-218.

753   23. Vikingsson GA. Energetic studies on fin and sei whales caught off Iceland. Rep. Int.

754   Whal. Commn. 1990; 40:365- 373.

755   24. Christiansen F, Vikingsson GA, Rasmussen MH, Lusseau D. Mike whales maximise

756   energy storage on their feeding grounds. J Exp Biol. 2013; 216: 427-436.

757   25. Lockyer CH, McConnel LC, Waters TD. Body condition in terms of anatomical and

758   biochemical assessment of body fat in North Atlantic fin and sei whales. Can J Zool.

759   1985; 63: 2328-2338.

760   26. Lambertsen RH. A biopsy system for large whales and its use for cytogenetics. J.

761   Mamm. 1987; 68: 443-445.

762   27. Ryan C, McHugh B, O'Connor I, Berrow S. Lipid content of blubber biopsies is not

763   representative of blubber in situ for fin whales (*Balaenoptera physalus*). Mar Mamm Sci.

764   2012; 29: 542-547.

765   28. Pettis HM, Rolland RM, Hamilton PK, Brault S, Kowlton AR, Kraus SD. Visual health

766   assessment of North Atlantic right whales (*Eubalaena glacialis*) using photographs. Can.

767   J. Zool. 2004; 82: 8-19.

768   29. Bradford AL, Weller, DW, Punt WAE, Ivashchenko YI, Burdin AM, VanBlaricom GR,

769   Brownell RL Jr. Leaner leviathans: body condition variation in a critically endangered

770   whale population. J Mammal. 2012; 93: 251-266.

771   30. Miller CA, Best PB, Perryman WL, Baumgartner MF, Moore MJ. Body shape changes

772   associated with reproductive status, nutritive condition and growth in right whales

773   *Eubalaena glacialis* and *E. australis*. Mar Ecol Prog Ser. 2012; 459: 135-156.

774   31. Durban JW, Moore MJ, Gustavo C, Hickmott LS, Bocconcelli A, Howes G, Bahamonde

775   PA, Perryman WL, LeRoi DJ. Photogrammetry of blue whales with an unmanned

776   hexacopter. Mar Mamm Sci. 2016; 32:1510-1515.

777   32. Moya-Laraño J, Macias-Ordóñez R, Blanckenhorn WU, And Fernández-Montraveta C.

778   Analysing body condition: mass, volume or density? J. Anim. Ecol. 2008; 77: 1099-

779   1108.

780   33. Williams TM, Davis RW, Fuiman LA, Francis J, LeBoeuf BJ, Horning M, Calambokidis

781   J, Croll DA. Sink or swim: strategies for cost-efficient diving by marine mammals.

782   Science. 2000; 288: 133-136.

783   34. Aoki K, Watanabe Y, Crocker DE, Robinson PW, Biuw M, Costa DP, Miyazaki N,

784   Fedak MA, Miller PJO. Northern elephant seals adjust gliding and stroking patterns with

785   changes in buoyancy: validation of at-sea metrics of body density. J Exp Biol. 2011;

786   214: 2973-2987.

787 35. Richard G, Vacquié-Garcia J, Jouma'a J, Picard B, Génin A, Arnould JPY, Bailleu F,

788   Guinet C. Variation in body condition during the post-moult foraging trip of southern

789   elephant seals and its consequences on diving behaviour. J Exp Biol. 2014; 217: 2609-

790   2619.

791 36. Nowacek DP, Johnson MP, Tyack PL, Shorter KA, McLellan WA, Pabst DA. Buoyant

792   balaenids: the ups and downs of buoyancy in right whales. Proc R Soc B. 2001; 268:

793   1811-1816.

794 37. Sato K, Mitani Y, Cameron MF, Siniff DB, Naito Y. Factors affecting stroking patterns

795   and body angle in diving Weddell seals under natural conditions. J Exp Biol. 2003; 206:

796   1461-1470.

797 38. Miller PJO, Johnson MP, Tyack PL, Terray EA. Swimming gaits, passive drag, and

798   buoyancy of diving sperm whales *Physeter macrocephalus*. J Exp Biol. 2004; 207:

799   1953-1967.

800 39. Watanabe Y, Baranov EA, Sato K, Naito Y, Miyazaki N. Body density affects stroke

801   patterns in Baikal seals. J Exp Biol. 2006; 209: 3269-3280.

802 40. Biuw M, Boehme L, Guinet C, Hindell M, Costa, D, Charrassin JB, Roquet F, Bailleul

803   F, Meredith M, Thorpe S, et al. Variations in behavior and condition of a Southern

804   Ocean top predator in relation to in situ oceanographic conditions. Proc. Natl. Acad. Sci.

805   2007; 104: 13705-13710.

806 41. Robinson PW, Simmons SE, Crocker DE, Costa DP. Measurements of foraging success

807   in a highly pelagic marine predator, the northern elephant seal. J Anim Ecol. 2010; 79:

808   1146-1156.

809 42. Crocker DE, Le Boeuf BJ, Costa DP. Drift diving in female northern elephant seals:

810   implications for food processing. Can. J. Zool. 1997; 75: 27–39. doi:10.1139/z97-004

811   43. Page B, McKenzie J, Goldsworthy SD. Inter-sexual differences in New Zealand

812   fur seal diving behaviour. Mar Ecol Prog Ser. 2005; 304: 249–264.

813   44. Andersen JM, Stenson GB, Skern-Maurizen M, Wiersma YF, Rosing-Asvid A, Hammill

814   MO, Boehme L. Drift diving by hooded seals (*Cystophora cristata*) in the Northwest

815   Atlantic Ocean. PLoS One. 2014. https://doi.org/10.1371/journal.pone.0103072

816   45. Reilly JJ, Fedak MA. Measurement of the body composition of living gray seals by

817   hydrogen isotope dilution. J Appl Physiol. 1990; 69: 885-891.

818   46. Piscitelli MA, McLellan WA, Rommel SA, Blum JE, Barco SG, Pabst DA. Lung size

819   and thoracic morphology in shallow- and deep-diving cetaceans. J Morphol. 2010; 271:

820   654-673.

821   47. Aoki K, Sato K, Isojunno S, Narazaki T, Miller PJO. High diving metabolic rate

822   indicated by high-speed ransit to depth in negatively buoyant long-finned pilot whales. J

823   Exp Biol. 2017; 220: 3802-3811.

824   48. Woodward BL, Winn JP, Fish FE. Morphological specializations of baleen whales

825   associated with hydrodynamic performance and ecological niche. J Morphol. 2006; 267:

826   1284-1294.

827   49. Johnson M, Tyack PL. A digital acoustic recording tag for measuring the response of

828   wild marine mammals to sound. IEEE J Ocean Eng. 2003; 28: 3-12.

829   50. Shiomi K, Narazaki T, Sato K, Shimatani K, Arai N, Ponganis PJ, Miyazaki N. Data-

830   processing artefacts in three-dimensional dive path reconstruction from geomagnetic and

831   acceleration data. Aquat Biol. 2010; 8:299-304.

832   51. Goldbogen JA, Pyenson ND, Shadwick RE. Big gulps require high drag for fin whale

833   lunge feeding. Mar Ecol Prog Ser. 2007; 349: 289-301.

834 52. Simon M, Johnson M, Madsen PT. Keeping momentum with a mouthful of water:

835 behaviour and kinematics of humpback whale lunge feeding. J Exp Biol. 2012; 215:

836 3786 – 3798.

837 53. Bose N, Lien J. Propulsion of a fin whale (*Balaenoptera physalus*): why the fin whale is

838 a fast swimmer. Proc R Soc Lond B. 1989; 237:175-200.

839 54. Lockyer C. Body weights of some species of large whales. J. Cons. Int. Explor. Mer.

840 1976; 36: 259-273.

841 55. Fish FE. Power output and propulsive efficiency of swimming bottlenose dolphins

842 (*Tursiops truncates*). J Exp Biol. 1993 185: 179-193.

843 56. Kooyman GL. Diverse Divers. Physiology and behaviour. Berlin: Springer-Verlag;

844 1989.

845 57. Brooks SP, Gelman A. General methods for monitoring convergence of iterative

846 simulations. J. Comput. Graph, Stat. 1998; 7: 434-455.

847 58. Ramp C, Delarue J, Palsbøll PJ, Sears R, Hammond PS. Adapting to a Warmer Ocean—

848 Seasonal Shift of Baleen Whale Movements over Three Decades. PLoS ONE, 2015; 10:

849 e0121374. doi: 10.1371/journal.pone.0121374

850 59. Sato K, Naito Y, Kato A, Niizuma Y, Watanuki Y, Charrassin JB, Bost CA, Handrich Y,

851 Le Maho Y. Buoyancy and maximal diving depth in penguins: do they control inhaling

852 air volume? J Exp Biol. 2002; 205: 1189-1197.

853 60. Miklosovic DS, Murray MM, Howle LE, Fish FE. Leading-edge tubercles delay stall on

854 humpback whale (*Megaptera novaeangliae*) flippers. Phys Fluids. 2004; 16: L39-L42.

855 doi: http://dx.doi.org/10.1063/1.1688341

856 61. Wiley D, Ware C, Bocconelli A, Cholewiak D, Friedlaender A, Thompson M, Weinrich

857 M. Underwater components of humpback whale bubble-net feeding behaviour.

858 Behaviour. 2011; 148: 576-602.

859   62. Fish FE, Battle JM. Hydrodynamic design of the humpback whale flipper. J Morphol.

860   1995; 225: 51-60.

861   63. Segre PS, Seakamela SM, Meyer MA, Findlay KP, Goldbogen JA. A hydrodynamically

862   active flipper-stroke in humpback whales. Curr Biol. 2017; 27: R623-R641.

863   64. Miller CA, Reeb D, Best PB, Knowlton AR, Brown MW, Moore MJ. Blubber thickness

864   in right whales *Eubalaena glacialis* and *Eubalaena australis* related with reproduction,

865   life history status and prey abundance. Mar Ecol Prog Ser. 2011; 438: 267-283.

866   65. Weinstein B, Friedlaender AS. Dynamic foraging of a top predator in a seasonal polar

867   marine environment. Oecologia. 2017; 185: 427-435.

868   66. Leith D, Lowe R. Mechanics of baleen whale lungs. Fed Proc. 1972; 31: 335A

869   67. Piscitelli MA, Raverty SA, Lillie MA, Shadwick RE. A review of cetacean lung

870   morphology and mechanics. J Morphol. 2013; 274: 1425-1440.

871   68. Ponganis PJ. Diving mammals. Compr Physiol. 2011; 1: 447-465.

872   69. Scholander PF. Experimental investigations on the respiratory function in diving

873   mammals and birds. Hvalradets skrifter. 1940; 22: 1-131.

874   70. Skrovan RC, Williams TM, Berry PS, Moore PW, Davis RW. The diving physiology of

875   bottlenose dolphins (*Tursiops truncatus*), part II: Biomechanics and changes in buoyancy

876   at depth. J Exp Biol. 1999; 202: 2749-2761.

877   71. Hain JHW, Carter GR, Kraus SD, May CA, Winn HE. Feeding behaviour of the

878   humpback whale, *Megaptera novaeangliae*, in the western north Atlantic. Fish Bull.

879   1982; 80: 259-268.

880   72. Tyack P, Whitehead H. Male competition in large groups of wintering humpback

881   whales. Behaviour, 1983; 83: 132–154.

882

883

Supporting Information

S1 Fig. Examples of linear regression of speed over time to estimate acceleration during 5s sub-glides. Linear regression of speed over time was conducted at each 5s sub-glide to estimate acceleration as a slope of the regression line. Top and bottom panels show examples from 3MPD3GT and DTAG deployments, respectively.

S1 File. Data of all 5-s sub glides performed by tagged humpback whales. This file includes all 5-s sub glides data used in this study.